Effect of carbon on interstitial ordering and magnetic properties of -Fe2(N,C)1-z

Brink, Bastian; Ståhl, Kenny; Christiansen, Thomas Lundin; Frandsen, Cathrine; Hansen, Mikkel Fougt; Beran, Pemysl; Somers, Marcel A. J.

Published in:
Journal of Alloys and Compounds

Link to article, DOI:
10.1016/j.jallcom.2016.09.317

Publication date:
2017

Document Version
Peer reviewed version

Effect of carbon on interstitial ordering and magnetic properties of ε-$Fe_2(N,C)_{1-z}$

Bastian K. Brink[a,c], Kenny Ståhl[b], Thomas L. Christiansen[a], Cathrine Frandsen[c], Mikkel Fougt Hansen[d], Přemysl Beran[e], Marcel A. J. Somers[a,*]

[a]Department of Mechanical Engineering, Technical University of Denmark, Produktionstorvet B425, DK-2800 Kgs. Lyngby, Denmark

[b]Department of Chemistry, Technical University of Denmark, Kemitorvet B206, DK-2800 Kgs. Lyngby, Denmark

[c]Department of Physics, Technical University of Denmark, Fysikvej B307, DK-2800 Kgs. Lyngby, Denmark

[d]Department of Micro- and Nanotechnology, Technical University of Denmark, Ørsteds Plads B345B, DK-2800 Kgs. Lyngby, Denmark

[e]Nuclear Physics Institute, Academy of Sciences of the Czech Republic, 250 68 Řež near Prague, Czech Republic

[*]somers@mek.dtu.dk

Abstract

Hexagonal ε-iron nitride and ε-iron carbonitride phases are formed on nitriding and nitrocarburizing of iron and steel surfaces and can exist in broad compositional ranges. Long-range nitrogen ordering and magnetic properties for ε-iron nitrides and their dependence on composition have been the focus of several studies. So far, limited

attention has been paid to the carbonitrides. In the current work, the effects of substitution of nitrogen by carbon on the interstitial ordering and magnetic properties in $Fe_2(C,N)_{1-z}$ are explored using neutron diffraction, Mössbauer spectroscopy and vibrating sample magnetometry. Neutron diffraction patterns showed 001 and 301 superstructure reflections, confirming a previously proposed structural model in space group $P\bar{3}1m$ (compared to $P6_322$ for the pure nitrides). On partial substitution of nitrogen by carbon in ε-iron nitride the Curie temperature, the saturation magnetization and the hyperfine fields of the iron atoms are increased, while isomer shifts are decreased. The effects on the *a* and *c* lattice parameters indicate a change in interstitial ordering, which is related to more favorable interactions between a nitrogen and carbon atom than among nitrogen atoms. This interaction leads to additional interstitial (short-range) ordering and a decrease in the *c* lattice parameter, while the *a* lattice parameter is largely unaffected.

Keywords: neutron diffraction, vibrating sample magnetometry, epsilon iron nitride, thermal expansion, interstitial order

1. Introduction

Scientific interest in ε-iron (carbo)nitride is derived from their metallurgical importance as these phases develop on iron and steel surfaces during thermochemical treatment by nitriding and nitrocarburizing [1]. The structure of ε-Fe_2N_{1-z} is based on an h.c.p. (hexagonal close-packed) iron lattice with nitrogen occupying octahedral interstitial sites. This configuration includes face-sharing octahedral sites. The simultaneous occupation of two of these neighboring sites induces strong repulsive

interactions. Hence, such a structural feature does not occur for any well-ordered interstitial compound [2]. This limits the maximum nitrogen content to the composition Fe_2N, which is unattainable in the ε-phase, because for this composition N atoms rearrange under the formation of the orthorhombically distorted ζ-Fe_2N [3].

For ε-Fe_2N_{1-z} in the compositional range of $0.01 \leq z \leq {}^1/_3$, Jack [4] derived a structural model for nitrogen ordering on the basis of superstructure reflections observed in X-ray diffraction patterns, requiring unit cell dimensions expanded by $3^{1/2} \times 3^{1/2} \times 1$ with respect to the h.c.p. cell. This structural model is based on ideally ordered structures Fe_3N ($z = {}^1/_3$) (or Fe_6N_2) in space group *P6₃22* and Fe_2N ($z = 0$) in space group *P$\bar{3}$1m* although only valid for $z \geq 0.01$, as noted. Thermodynamic models based on repulsive pairwise interaction of interstitial atoms also predict these ground structures [5,6]. The intermediate range is described by *P312* symmetry. The superstructure cell contains six Fe atoms and six octahedral interstitial sites. The main difference between the space groups is the number of inequivalent octahedral sites, which is three for space group *P6₃22*, four for *P$\bar{3}$1m* and six for *P312*. Sites are labeled A1-C2 according to Table 2 [7] and the structures are shown in Figure 1. Starting from a composition of Fe_3N, the sites A1 and B2 are preferentially filled. Increasing nitrogen content fills the C2 site.

Table 1: Site occupancies (ρ), Wyckoff sites (Wyc.) and coordinates (r) for octahedral sites in ε-Fe_2N_{1-z} according to the model of Jack [4].

	ε-Fe_3N - *P6₃22*			ε-Fe_2N_{1-z} - *P312*			ε-Fe_2N - *P$\bar{3}$1m*		
Site	ρ	Wyc.	r	ρ	Wyc.	r	ρ	Wyc.	r
A1	1	(2*c*)	$({}^1/_3,{}^2/_3,{}^1/_4)$	1	(1*a*)	(0,0,0)	1	(1*a*)	(0,0,0)
A2	0	(2*d*)	$({}^1/_3,{}^2/_3,{}^3/_4)$	0	(1*b*)	$(0,0,{}^1/_2)$	0	(1*b*)	$(0,0,{}^1/_2)$
B1	0	(2*d*)	$({}^2/_3,{}^1/_3,{}^1/_4)$	0	(1*c*)	$({}^1/_3,{}^2/_3,0)$	0	(2*c*)	$({}^1/_3,{}^2/_3,0)$

B2	1	(2*c*)	($^2/_3$,$^1/_3$,$^3/_4$)	1	(1*d*)	($^1/_3$,$^2/_3$,$^1/_2$)	1	(2*d*)	($^1/_3$,$^2/_3$,$^1/_2$)
C1	0	(2*b*)	(0,0,$^1/_4$)	0	(1*e*)	($^2/_3$,$^1/_3$0)	0	(2*c*)	($^2/_3$,$^1/_3$,0)
C2	0	(2*b*)	(0,0,$^3/_4$)	1-3*z*	(1*f*)	($^2/_3$,$^1/_3$,$^1/_2$)	1	(2*d*)	($^2/_3$,$^1/_3$,$^1/_2$)

The different space groups, and thus the nitrogen ordering, can be distinguished in terms of superstructure reflections observed in diffraction experiments. For ε-type structures this information is contained in four different classes of reflections named after the first occurring representative reflection [7]:

(110) type: $h - k = 3n$, l even

(001) type: $h - k = 3n$, l odd

(100) type: $h - k \neq 3n$, l even

(101) type: $h - k \neq 3n$, l odd

where n is an integer. The (110) type is always fundamental with respect to the ideal h.c.p. arrangement of the metal atoms. The overall structure factor is the sum of metal and interstitial contributions. The types (100) and (101) are pure superstructure reflections, i.e. for an undistorted h.c.p. metal only interstitials contribute to the structure factor. For the type (001) reflections there is no metal contribution if $h, k = 3n$, e.g. 001, 003, 301 and 331.

From Jack's *P312* model, superstructure reflections of the types (101), (100) and (001) are expected. Leineweber *et al.* [8] investigated ε-Fe_2N_{1-z} in the compositional range $0.07 \leq z \leq 0.27$, but only observed (001) reflections for $Fe_2N_{0.81}$[1]. Other samples

[1] This composition reflects the $Fe_{24}N_{10}$ composition for which Jack [4] proposed a special ordering. This ordering could not be confirmed.

were modeled in *P6*$_3$*22* symmetry in which the (001) type is systematically extinct. Partial occupancy of the 2*b* site was found, and this deviates from the ideal model in that also site C1 will be partially occupied. The ε-nitrides become increasingly disordered at elevated temperatures. For a composition close to Fe_3N reversible disorder is observed above 470 K as nitrogen is partially transferred to the 2*b* Wyckoff site [9]. Additionally, it has been shown that the degree of disorder can be coupled to the axial ratio *c*/*a* [10]. With increasing nitrogen content the Curie temperature decreases from $T_C \simeq 575$ K for $z = {}^1/_3$ to $T_C \simeq 10$ K for $z = 0.01$ [9,11].

Iron sites in ε-Fe_2N_{1-z} can be differentiated with respect to the number of nearest neighboring nitrogen atoms using Mössbauer spectroscopy [12]. An overview of published Mössbauer data for the iron nitrides is available in Ref. [13]. According to the ground state structure each iron atom should be surrounded by two nitrogen atoms for $z = {}^1/_3$. For increasing nitrogen content an increasing number of iron atoms is surrounded by three nitrogen atoms. Experimentally, two separate iron environments, each characterized by three nitrogen nearest neighbors, are observed [14,15], which may not readily be explained by the model.

Shang *et al.* [16] proposed an explanation for the two distinct iron environments with 3 N nearest neighbors, based on simultaneous occupation of the A1, B1 and C1 (or equivalently A2, B2 and C2) sites, i.e. the top (or bottom) plane of the trigonal prisms comprised of octahedral interstitial sites (cf. Fig. 1). This configuration also avoids octahedral sites sharing common faces, but is energetically unfavorable due to the shorter distances between the mutually repelling nitrogen atoms. The discrepancy between experimental and calculated values of hyperfine interactions [16] and lack of additional experimental evidence for this type of ordering do not support this

description. A simple explanation was offered by Chen *et al.* [14] involving, for each iron atom with three nitrogen nearest neighbors, the iron atoms in the second coordination shell, which can be predominantly surrounded by either two or three nitrogen atoms, causing the two hyperfine fields for iron atoms with three nitrogen neighbors.

In ε-iron nitrides, nitrogen atoms can in principle be replaced by carbon atoms. The structure is similar to that of the pure nitrides [17], but so far limited research has been performed on the resulting structural modifications. It has been reported that the axial ratio *c*/*a* decreases with increasing carbon content [18]. In the investigation of a carbonitride with composition $Fe_2(N_{0.8}C_{0.20})_{0.92}$, type (001) reflections were observed without the presence of type (100) reflections [8]. Although allowed by symmetry, a situation where (100) reflections are not present is expected for ε-Fe_2N and a structural model in space group $P\bar{3}1m$ was chosen. However, no extended conclusion regarding the interstitial ordering in the ε-carbonitrides can be drawn from this single observation. Detailed information about the interstitial ordering in ε-iron carbonitrides is difficult to obtain with X-ray diffraction due to the low scattering power of nitrogen and carbon compared to iron. Light atoms may, however, contribute strongly to the diffracted intensity of neutrons, even in the presence of heavier atoms. The comparable nuclear scattering lengths of iron, nitrogen and carbon [19] enable a more accurate determination of interstitial occupancies. Even for the pure nitrides, the ordering of nitrogen is not completely understood, with apparent additional ordering occurring for the composition $Fe_2N_{0.81}$ and additional diffuse scattering observed in electron diffraction patterns for higher nitrogen contents [8,20]. In order to investigate the interstitial ordering in ε-iron (carbo)nitrides, samples with different nitrogen and carbon contents were synthesized and the structural and magnetic properties were characterized

using neutron diffraction, vibrating sample magnetometry (VSM) and Mössbauer spectroscopy.

2. Experimental

Iron powder (99.0+% purity, Goodfellow Cambridge Ltd.) with a mean particle size of 6 – 8 μm was used for nitriding and nitrocarburizing with ammonia, nitrogen and hydrogen gasses of 99.999% and propene of 99.5% purity. Four samples were prepared in ceramic crucibles in a Netzsch STA 449 C Jupiter thermal analyzer at 718 K for 2.5 – 3 hours. Total flow rates of 55 – 68 mL/min were used with a constant N_2 flow of 5 mL/min for protection of electronics in the measurement compartment. In order to obtain sufficient amounts for all analyses, ten identical batches were combined to form each sample.

The compositions determined by combustion infrared detection (carbon content) on a LECO CS230 and by inert gas fusion thermal conductivity detection (nitrogen content) on a LECO TN500 is given in Table 2. The determined composition of $Fe_2(N_{0.757}C_{0.243})_{0.84}$ was corrected for the presence of small amounts (1.3% by mass) of γ'-Fe_4N in the sample, assuming stoichiometric composition and zero carbon content in the latter.

Table 2: Applied gas flow rates (mL/min), corresponding activities[†] of N and C (a_N and a_C with respect to N_2 and graphite at 1 bar, respectively) and resulting sample compositions for samples synthesized at 718 K.

NH_3	H_2	C_3H_6	N_2	a_N	a_C	Composition
50	-	-	5	∞	0	$Fe_2N_{0.91}$
50	7	-	5	3551	0	$Fe_2N_{0.72}$
50	8	3	5	2906	1109	$Fe_2(N_{0.757}C_{0.243})_{0.84}$
50	4	3	5	8220	1398	$Fe_2(N_{0.819}C_{0.181})_{0.88}$

[†]Activities are calculated using thermodynamic data given in references [21] and [22].

Two additional samples were prepared in a semi-industrial LAC PKRC55/09 furnace retrofitted for nitriding/nitrocarburizing at 693 K. The applied gas flow rates and calculated sample compositions are given in Table 3. Very similar sample compositions were obtained with a slightly higher carbon content for the highest applied propene flow rate of 19 mL/min.

An Agilent SuperNova diffractometer with an Atlas S2 CCD detector using Mo K_α radiation and calibrated with a LaB_6 standard was used for the determination of lattice parameters for $Fe_2N_{0.72}$.

Neutron powder diffraction on the samples given in Table 3 was performed using the MEREDIT diffractometer at the Nuclear Physics Institute ASCR in Řež, the Czech Republic. Samples were placed in vanadium containers with a diameter of 13 mm, and a monochromator consisting of three mosaic Cu(220) crystals provided a neutron wavelength of λ = 1.46 Å. Data were collected at room temperature in a 2θ range of 4 – 144° with a step size of 0.08° in 2θ.

Table 3: Gas flow rates of ammonia and propene, treatment time and resulting sample composition of the samples synthesized at 693 K[†].

NH_3 [L/min]	C_3H_6 [mL/min]	Time [hours]	Composition
1	11	80	$Fe_2(N_{0.715}C_{0.285})_{0.92}$
1	19	55	$Fe_2(N_{0.706}C_{0.294})_{0.92}$

[†]No nitrogen and carbon activities can be obtained from the inlet gas composition, because the H_2 content is unknown. Generally, abundant dissociation of gas species occurs at the surfaces in the furnace.

Additional neutron diffractograms were collected using the E3 diffractometer at Helmholtz-Zentrum Berlin (HZB), Germany [23]. Samples were placed in vanadium containers with a diameter of 8 mm under vacuum and data collected at room

temperature, 373 K, 473 K and 573 K with a neutron wavelength of λ = 1.4892 Å. The applied wavelength and correction for diffraction angle (2θ) zero shift was determined from a Cu powder standard. Data were collected in a 2θ range of 40 – 103° with a step size of 0.105° in 2θ. Rietveld refinements of intensity versus scattering angle (2θ) were carried out using the program WINPOW, a local variation of LHMP [24]. Pseudo-Voigt profile functions were applied together with Chebyshev background polynomials.

Vibrating sample magnetometry was performed with a Lake Shore Cryotronics 7400 Series Vibrating Sample Magnetometer (VSM) equipped with either a single-stage variable temperature option (model 74035) or a low-temperature variable temperature cryostat (model 74018).

^{57}Fe Mössbauer spectra were recorded using conventional constant acceleration spectrometers with sources of ^{57}Co in Rh on samples mixed with boron nitride powder. Spectra obtained at low temperatures were recorded in a closed cycle helium refrigerator (APD Cryogenics) and isomer shifts are given with respect to α-Fe at room temperature. Mössbauer spectra were fitted with Lorentzian line profiles and sextets were constrained to an intensity ratio of 3:2:1:1:2:3 and pairwise equal line widths.

3. Results and Discussion

3.1 Magnetic properties

Hysteresis curves and the specific magnetization as a function of temperature for the ε-(carbo)nitrides show a clear variation in the saturation value, σ_s, of the specific magnetization and the Curie temperature, T_C, with changing interstitial content (Fig. 2 and Table 4). Except for $Fe_2N_{0.91}$, the saturation specific magnetization measured at 80 K in an applied field of B_0 = 1.6 T decreases for increasing interstitial content. A similar

trend is noticed for the Curie temperatures, taken as the zero-point of the second derivative of the magnetization curves [25]. Below the Curie temperature all samples can be classified as soft ferromagnets (coercivities around 5 mT at 80 K). The reduction of σ_s and T_C values with increasing interstitial content is well-known for ε-iron nitride [8,26,27]. The observed variation in magnetic properties can be explained from changes in the electronic band structure, which includes hybridization of the 2*p* states of C/N and the Fe 3*d* states [28–31]. Increasing the interstitial content increases the number of electrons in the partially filled band of minority spins. Consequently, the difference between majority and minority spins is reduced and the magnetic moment of Fe is lowered.

Substitution of nitrogen by carbon has in one case been shown to cause an increase in both magnetization and Curie temperature [8]. This is consistent with the interaction between C/N 2*p* and Fe 3*d* states, because carbon has only two 2*p* electrons while nitrogen has three 2*p* electrons. Hence, replacing nitrogen by carbon is associated with fewer electrons in Fe 3*d* band and thus a higher saturation magnetization and Curie temperature.

Table 4: Curie temperature (T_C) and specific saturation magnetization (σ_s) at 80 K in an applied field of B_0 = 1.6 T determined for ε-iron (carbo)nitrides.

Sample	$Fe_2N_{0.72}$	$Fe_2(N_xC_{1-x})_{0.84}$	$Fe_2(N_xC_{1-x})_{0.88}$	$Fe_2(N_xC_{1-x})_{0.92}$	$Fe_2(N_xC_{1-x})_{0.92}$	$Fe_2N_{0.91}$
x	-	0.757	0.819	0.706	0.715	-
σ_s [Am^2/kg]	154	132	114	103	101	71
T_C [K]	480	431	349	340	336	222

The dependence of the Curie temperature on interstitial content is shown in Fig. 3 and compared to literature data. The T_C values determined for the two investigated ε-nitride samples agree with published literature values. Evidently, the ε-carbonitride

samples have a higher T_C than the ε-nitrides for the same total interstitial content. In this respect, the present results confirm an earlier single observation of increased magnetization and Curie temperature for ε-iron carbonitrides as compared to ε-iron nitrides of comparable total interstitial content [8], as a general trend.

3.2 Mössbauer spectroscopy

The presence of magnetic ordering at low temperatures is confirmed by Mössbauer spectroscopy. Each individual spectrum recorded at 18 K (Fig. 4) could be fitted with a combination of three sextets. The sextet components correspond to Fe surrounded by one (I), two (II) or three (IIIa and IIIb) nitrogen or carbon atoms [14,15]. In the ideal structure of ε-Fe_3N only component II should be observed, but increasing nitrogen or carbon contents, $z < {}^1/_3$ for ε-$Fe_2(N,C)_{1-z}$, lead to some iron atoms having three N/C nearest neighbors. Four nearest neighbors are not observed due to the repulsive nature of the interactions of simultaneously occupied face-sharing octahedral positions.

The sextet corresponding to just one nitrogen nearest neighbor was only observed for the sample with the lowest interstitial content: $Fe_2N_{0.72}$ (Table 5). This configuration develops due to partial disordering from the ground state structure according to the reaction 2 (II) → (I) + (III) [8,14]. The fractional occupancy of interstitials per two iron atoms (=1-z) for ε-$Fe_2(N,C)_{1-z}$ can be calculated as $\Sigma(f_i \cdot i)/3$, where f_i is the relative area of sextets corresponding to iron atoms surrounded by i = 1, 2 or 3 interstitial atoms.

The calculated values slightly overestimate the total interstitial content as determined by combustion analysis. The systematic deviation could have its origin in either the chemical analysis of the samples or the fitting procedure of Mössbauer spectra. The largest deviation (6 %) is observed for $Fe_2N_{0.72}$ and is likely the result of a

less than accurate fit of the minority component corresponding to one nitrogen nearest neighbor. Additional deviations (up to 2 % for the remaining samples) are expected from the simplification of fitting individual sextets to components that are actually characterized by a distribution in hyperfine fields. This is evident from broadening of spectral lines, and particularly the component corresponding to three interstitial nearest neighbors requires (at least) two sextets (IIIa and IIIb) in order to obtain reasonable fits. This is in accordance with the interpretation given by Chen *et al*. [14] who attribute the observation to variations in the second coordination shell. The presence of N and/or C further complicates the picture, because it will also lead to differences in the first coordination shell, depending on the number of nitrogen/carbon among the total number of interstitials. Line widths in excess of 1 mm/s are observed compared to an instrumental broadening of approximately 0.25 mm/s, which confirm that a distribution of hyperfine fields is involved. In research on the pure nitrides, where the sextet corresponding to three nitrogen atoms was not resolved in two distinct components, broad lines were also encountered for the component corresponding to two nitrogen neighbors [32,33]. This is similar to the observations of Chen *et al.* when using only one sextet for component III and may hint that a distribution is also the appropriate description for component II.

The entire distribution in hyperfine fields presumably depends on the various configurations around neighboring iron atoms. So far, first principles calculations of hyperfine interactions have focused on fully ordered systems without contributions from possible configurations of surrounding iron atoms [16]. This limits the possibility for a quantitative interpretation of the distributions, and the individual components typically fitted for the ε-nitrides were therefore used as an approximation.

Table 5: Hyperfine field (B_{hf}), isomer shift (δ) and relative contribution (f_i) of sextets designated I, II, IIIa and IIIb fitted to Mössbauer spectra of ε-$Fe_2(N,C)_{1-z}$ powder samples recorded at 18 K. $\Sigma(f_i \cdot i)/3$ is the fractional occupancy of interstitials per two iron atoms (= 1-*z*) as calculated from the relative contributions of iron atoms surrounded by i = 1, 2 or 3 interstitial atoms.

	Sample	$Fe_2N_{0.72}$	$Fe_2(N_{1-x}C_x)_{0.84}$	$Fe_2(N_{1-x}C_x)_{0.88}$	$Fe_2(N_{1-x}C_x)_{0.92}$	$Fe_2(N_{1-x}C_x)_{0.92}$	$Fe_2N_{0.91}$
	x	-	0.243	0.181	0.294	0.285	-
I	B_{hf} [T]	33.8	-	-	-	-	-
	δ [mm/s]	0.41	-	-	-	-	-
	f [%]	0.8	-	-	-	-	-
II	B_{hf} [T]	26.2	26.2	26.2	25.9	25.7	25.5
	δ [mm/s]	0.47	0.46	0.47	0.46	0.46	0.50
	f [%]	71.2	41.1	31.7	18.5	17.5	21.0
IIIa	B_{hf} [T]	14.4	16.0	15.4	16.4	15.9	13.4
	δ [mm/s]	0.53	0.51	0.52	0.50	0.50	0.56
	f [%]	28.0	49.5	49.9	34.4	38.2	31.9
IIIb	B_{hf} [T]	-	12.2	11.7	13.0	12.7	7.7
	δ [mm/s]	-	0.59	0.56	0.52	0.52	0.56
	f [%]	-	9.4	18.4	47.1	44.3	47.1
	$\Sigma(f_i \cdot i)/3$	0.76	0.86	0.89	0.94	0.94	0.93

Values of the hyperfine fields (B_{hf}) and isomer shifts (δ) obtained from the fits are collected in Table 5. The quadrupole shifts were small and the quality of the fits was not reduced if the quadrupole shifts were constrained to zero, in agreement with the results of Chen *et al*. [14]. These values are therefore not tabulated. Hyperfine fields and isomer shifts are compared to values for ε-Fe_2N_{1-z} in Fig. 5. Hyperfine fields for the ε-carbonitrides are consistently higher than for the ε-nitrides of the same total interstitial content, which again is in agreement with the magnetization measurements and the explanation given on the basis of the electronic band structure.

The reduced isomer shifts of the ε-carbonitrides is similar to (calculated) effects of replacing nitrogen with carbon in Fe_4N, which can be interpreted in terms of an increased 4*s* electron density due to the lower electronegativity of C compared to N or a decreased screening effect of 3*d* electrons [34]. It is noted that the trend is not apparent

for component IIIb, which also displays significantly scattered literature values. This is most likely caused by the difficulty in fitting overlapping components and the discussed distributions in hyperfine fields, as opposed to well-defined sextets.

3.3 Neutron diffraction

Fig. 6 shows neutron diffractograms recorded using the diffractometer MEREDIT@NPI for the two samples with the highest carbon content of the studied compositions: $Fe_2(N_{0.706}C_{0.294})_{0.92}$ and $Fe_2(N_{0.715}C_{0.285})_{0.92}$. In both cases, type (001) superstructure reflections were observed, which are systematically extinct for space group *P6₃22*. Additional reflections, which coincide with the superstructure reflections, are present due to a small $^{\lambda}/_{2}$-contribution (with 0.4% intensity of the primary neutron wavelength, λ) from the applied monochromator. For space group *P6₃22*, the $^{\lambda}/_{2}$-contribution cannot entirely explain the observed intensities (Fig. 6*c-f*). The presence of type (001) superstructure reflections and thus the *P$\bar{3}$1m* structural model for the ε-carbonitrides confirms the suggestion by Leineweber *et al.* [8].

A comparison of the structural models shows that proceeding from space group *P6₃22*, with Wyckoff positions 2*b* and 2*c* occupied, to space group *P$\bar{3}$1m*, with occupation of 1*a* and 2*d*, corresponds to an increase in the degree of long range order. The structure of ε-Fe_2N_{1-z} described in space group *P6₃22* leads to occupation of Wyckoff site 2*b* (i.e. C1 and C2, cf. Table 1 and Figure 1) for $z < {}^{1}/_{3}$ [8]. Since simultaneous occupation of neighboring C1 and C2 sites is not likely to occur, as this is the shortest distance between octahedral sites, the structure will lead to short range ordering. For the ε-carbonitrides in space group *P$\bar{3}$1m* short range ordering is not necessary if only positions 1*a* and 2*d* are occupied.

Refinements were carried out with fixed C/N ratios at each site and the total number of interstitials was constrained to the nitrogen and carbon contents determined with combustion analysis. Refined C/N occupancies are listed in Table 6. For Wyckoff positions 1*b* and 2*c* occupancies refined to slightly negative values and were consequently fixed to zero.

Table 6: Lattice parameters (*a* and *c*), combined occupancy of Wyckoff sites by nitrogen and carbon (ρ), profile residual (R_p) and goodness-of-fit value (χ^2) obtained from Rietveld refinements. Neutron diffraction experiments at λ=1.46 Å.

Sample	$Fe_2(N_{0.706}C_{0.294})_{0.92}$	$Fe_2(N_{0.715}C_{0.285})_{0.92}$
a [Å]	4.7813(2)	4.7830(2)
c [Å]	4.4019(1)	4.4020(1)
$\rho(1a)$	0.882(10)	0.994(13)
$\rho(2c)$	0.070 (4)	0.122 (4)
$\rho(2d)$	0.876 (2)	0.767 (4)
R_p [%]	4.17	3.75
χ^2	9.26	5.40

The replacement of a minor amount of nitrogen by carbon at total interstitial content is seen to noticeably affect the refined occupancies; a slight increase in carbon content causes a more even distribution of interstitials, $\rho(1a) \approx \rho(2d)$. It should be realized that this result was obtained under the assumption of a fixed N/C ratio at each interstitial position. Below it is discussed that this is unlikely to be the case. Furthermore, it should be realized that the treatment times for synthesis of these samples were markedly different (cf. Table 3) and that thermal history may affect interstitial ordering [35]. Nevertheless, the most pronounced ordering was found in the sample that was treated for the shortest time (55 h). It is anticipated that ordering will become stronger with

treatment time. Hence, the difference in ordering is attributed to the difference in carbon content.

The neutron diffractograms recorded at the E3 diffractometer at HZB (not shown) have a lower signal/noise ratio and a limited 2θ range as compared to those shown in Fig. 6. As a consequence, the refined occupancies did not yield consistent results. Although reliable occupancies were not obtained, refinements indicated increased disorder at elevated temperatures as evidenced by an increase of the occupancy of Wyckoff site 2*d* for $Fe_2N_{0.91}$ (*P6*$_3$*22*) and 2*c* for the carbonitrides ($P\bar{3}1m$). Lattice parameters obtained for the two data sets are consistent as seen from comparing the values for $Fe_2(N_{0.706}C_{0.294})_{0.92}$ and $Fe_2(N_{0.715}C_{0.285})_{0.92}$ listed in Tables 6 and 7.

Thermal expansion of lattice parameters *a* and *c* is observed to be approximately linear up to the maximum investigated temperature of 573 K and can be satisfactorily fitted to the expression; $a(T) = a_{Tr}[1 + \alpha(T\text{-}T_r)]$, where *a* is the lattice parameter of the unit cell and a_{Tr} is the lattice parameter at a chosen reference temperature, T_r (Fig. 7). Room temperature lattice parameters and expansion coefficients are given in Table 7 and exhibit the following general trends: Increasing the total interstitial content (both N and C) increases both the *a* lattice parameter and thermal expansion within the basal plane of the hexagonal unit cell, although the sample containing only nitrogen, $Fe_2N_{0.91}$, deviates from this trend. A more complicated behavior is observed for the *c* lattice parameter and the thermal expansion perpendicular to the basal plane.

Table 7: Lattice parameters (*a* and *c*) at room temperature and expansion coefficients in terms of the lattice parameters and unit cell volume (*V*) for ε-iron (carbo)nitrides.

Sample	$Fe_2(N_{1-x}C_x)_{0.84}$	$Fe_2(N_{1-x}C_x)_{0.88}$	$Fe_2(N_{1-x}C_x)_{0.92}$	$Fe_2(N_{1-x}C_x)_{0.92}$	$Fe_2N_{0.91}$
x	0.243	0.181	0.294	0.285	-
a(RT) [Å]	4.7630(7)	4.7723(5)	4.7812(3)	4.7829(2)	4.7768(4)
c(RT) [Å]	4.4000(4)	4.4060(3)	4.4014(2)	4.4027(2)	4.4160(3)

$\alpha(a)$ [$\times 10^{-5}$ K^{-1}]	1.23 (3)	1.65 (2)	1.84 (8)	1.87 (7)	2.56(11)
$\alpha(c)$ [$\times 10^{-5}$ K^{-1}]	1.87(13)	1.70(10)	1.62 (6)	1.45 (4)	1.71 (8)
$\alpha(V)$ [$\times 10^{-5}$ K^{-1}]	4.35(17)	5.02(12)	5.32(15)	5.21(15)	6.87(31)

Since most of the samples investigated in this work have their Curie temperature above room temperature, contributions from magnetic ordering in neutron diffractograms are expected. For the ε-(carbo)nitrides nuclear and magnetic reflections coincide, but some disagreement persists regarding the alignment of the magnetic moments (within [8,9] or perpendicular [36,37] to the basal plane). Several magnetic models were attempted in analyzing the current data, but magnetic structures could not be resolved and were therefore not included in Rietveld refinements.

4 General Discussion

All lattice parameters for ε-$Fe_2(N,C)_{1-z}$ are plotted versus total interstitial content (1-*z*) in Fig. 8(*a*) and compared to additional values obtained with X-ray diffraction [38]. Within experimental accuracy the *a* lattice parameter corresponds to published relations for pure ε-nitrides [15,35] and ε-carbonitrides [39], while there are significant deviations for the *c* lattice parameter. These deviations from the relation for ε-nitrides increase with increasing carbon content. A reduced compositionally induced expansion in the *c* lattice parameter, while the *a* lattice parameter is mostly unaffected contradicts the early results obtained by Jack [17], where reductions in both *a* and *c* lattice parameters were observed for partial substitution of nitrogen by carbon. However, the current observations support the later findings of Naumann & Langenscheid [18].

Based on the published relation between lattice parameter *c* and interstitial content for ε-Fe_2N_{1-z} [15], c [Å] = 4.2723 + 0.159(1-*z*), a correction term has to be included to account for the fraction of interstitial carbon atoms, *x*, in ε-$Fe_2(N_{1-x}C_x)_{1-z}$. A least squares

fit to the current data yields a value for the correction term of –0.057(6) Å, resulting in the following relation for *c*:

$$c\ [\text{Å}] = 4.4313 - 0.159z - 0.057x \quad (1)$$

This fit does not completely describe the changes in lattice parameter for the carbonitrides, but is a significant improvement of the relation applicable for ε-nitrides as evident from Fig. 8(*b*).

The anisotropic effect on lattice parameters by substituting N with C suggests that carbon does not randomly substitute nitrogen, but rather has preferred crystallographic sites. This cannot be directly verified from the refined occupancies since Rietveld refinements were carried out with a fixed N/C ratio at each interstitial position. Rather, it can be deduced from the nature of the compositionally induced lattice expansion since edge-sharing contacts of octahedral interstitial positions occur exclusively parallel to (001). Simultaneous occupation of these positions causes repulsive interactions, which are accommodated by preferential expansion of the structure in the direction perpendicular of the basal plane of the hexagonal unit cell. For an ideal structure described in space group $P\bar{3}1m$, only Wyckoff sites 1*a* and 2*d* are occupied, corresponding to sites designated A1, B2 and C2 (cf. Table 1). Edge-sharing contacts occur between B2 and C2 (2*d*). Since the lattice parameter *a* is comparable for ε-nitrides and ε-carbonitrides it is deduced that these sites are preferentially occupied by nitrogen.

The expansion within the basal plane of the hexagonal unit cell is primarily governed by occupation of site A1 (1*a*). For preferred carbon occupancy of this site, a reduced lattice parameter *c* can be conceived as a result of less repulsive C-N interactions compared to N-N. For an ordered configuration in which nitrogen fully

occupies 2*d* and carbon 1*a*, each nitrogen atom is surrounded by three nearest neighbor N atoms in directions parallel to (001). Carbon, on the other hand, is surrounded by twelve nearest neighboring N atoms, albeit separated by a slightly larger distance (by a factor of approximately 1.3). The structure may thus be considered the result of maximizing the number of favorable C-N interactions. It may be argued that this result contrasts observations on annealing Fe-C-N martensite below 450 K, where a preliminary redistribution of interstitials into carbon-rich and nitrogen-rich regions occurs before precipitation of α"-$Fe_{16}N_2$ nitride and ε/η carbides [40,41]. It should be realized that Fe-N-C martensite is a (strongly) supersaturated solid solution of N and C in b.c.c. (body-centered cubic) Fe. As b.c.c. Fe essentially has a very low solubility for both N and C, the high interstitial content trapped by fast cooling of Fe-N-C austenite leads to a severely strained lattice, which, due to the asymmetric octahedral interstices, becomes b.c.t. (body-centered tetragonal). The development of α"-$Fe_{16}N_2$ could crystallographically be considered a consequence of the ordering of N atoms over interstitial sites in the b.c.t. Fe lattice. The total interstitial content in martensite is low as compared to the interstitial contents in the ε phase investigated here. For a face-centered cubic sublattice of Fe strict ordering of N atoms as in γ'-Fe_4N_{1-x} is observed with very low solubility for C. As compared to martensite, the interstitial solution of N and C in the h.c.p. iron sublattice of the ε phase is not supersaturated and the contents are so high that long range order of the interstitials does occur. It may therefore be suggested that the favorable C-N interactions observed here for high interstitial contents are exclusive for the h.c.p. arrangement of Fe atoms in ε-carbonitride, because both ε nitride and ε carbide are known phases.

The variation in interstitial ordering is also evident from the effects on the coefficients of thermal expansion. The ratio of expansion coefficients in *a* and *c*

directions from Table 7 is shown as a function of the total interstitial content per 2 Fe atoms in Fig.9. It has previously been demonstrated that variations in the *c*/*a* ratio at elevated temperature can be interpreted in terms of thermal disorder [42]. Disordering leads to an increased number of edge-sharing contacts. Both increasing disorder and increasing interstitial content thus cause a preferential expansion of the structure parallel to (001) planes. Increasing the total interstitial content will therefore tend to reduce the ratio of expansion coefficients $\alpha(c)/\alpha(a)$, in accordance with Fig. 9. Higher ratios are observed for higher carbon contents due to the favorable C-N interactions. In this respect it is important to realize that generally for higher temperature (and high interstitial content) the samples are in a paramagnetic state, while for low temperatures ferromagnetism may prevail, particularly for a low total interstitial content (cf. Fig. 2*b*). For the ε-nitrides, the axial ratio *c/a* exhibits a maximum around the Curie temperature [42] and a similar result is obtained for the current samples of ε-carbonitrides on evaluating the axial ratios from the values presented in Fig. 7. Evaluation of the expansion coefficients exclusively above T_C (i.e. in the paramagnetic state) does, however, not change the qualitative results presented in Fig. 9. This suggests that, although the magnetic state does affect the lattice parameters, the direct effects of variations in interstitial contents of nitrogen and carbon atoms dominate.

7. Conclusions

Partial substitution of nitrogen by carbon in ε-iron nitride affects both magnetic and structural properties. Trends in magnetic properties are consistent with available calculations on the electronic band structure in which hybridization occurs between the 2*p* states of C/N and the Fe 3*d* states. Curie temperatures, magnetization and hyperfine

fields are increased, while isomer shifts of iron are decreased in the carbonitrides, since carbon has only two 2*p* electrons whereas nitrogen has three.

The two components identified in Mössbauer spectra corresponding to iron atoms surrounded by three interstitials (IIIa and IIIb) should be interpreted as an approximation for the distribution in hyperfine fields caused by both the number and configuration of interstitial atoms around neighboring iron atoms.

The carbonitrides are described in space group $P\bar{3}1m$ as opposed to $P6_322$ for the pure nitrides, evidenced by the presence of type (001) superstructure reflections. The thresholds in both total interstitial content and carbon content that must be exceeded in order to change the symmetry have not been investigated. Changes in interstitial ordering are deduced from the observed effects on lattice parameters. Favorable C-N interactions (compared to N-N) lead to additional ordering and a decrease in the lattice parameter *c* while *a* is largely unaffected. These effects are also apparent for the anisotropic thermal expansion.

Acknowledgements

The Danish Council for Independent Research (DFF) is gratefully acknowledged for financial support under Grant 11-106293. This research project has been supported by the European Commission under the 7th Framework Programme through the 'Research Infrastructures' action of the 'Capacities' Programme, CP-CSA_INFRA-2011-1.1.17 Number 233883 NMI3 II. Support from the CANAM infrastructure (MSMT project no. LM2011019) of the NPI ASCR Rez is also greatly acknowledged. The authors are grateful to Danscatt for additional financing of travel expenses and to Robert C. Wimpory at HZB for assistance in collecting neutron diffraction data with the E3 diffractometer at BER II.

References

[1] A. Fry, Stickstoff im Eisen, Stahl und Sonderstahl. Ein neues Oberflächenhärtungsverfahren, Stahl Eisen. 43 (1923) 1271–1279.

[2] E. Parthé, K. Yvon, On the crystal chemistry of the close packed transition metal carbides. II. A proposal for the notation of the different crystal structures, Acta Crystallogr. B. 26 (1970) 153–163.

[3] K.H. Jack, Binary and ternary interstitial alloys. I. The iron-nitrogen system: The structures of Fe_4N and Fe_2N, Proc. R. Soc. London A. 195 (1948) 34–40.

[4] K.H. Jack, The iron–nitrogen system: The crystal structures of ε-phase iron nitrides, Acta Crystallogr. 5 (1952) 404–411.

[5] M. Hillert, M. Jarl, A regular-solution model for interstitial solutions in HCP metals, Acta Metall. 25 (1977) 1–9.

[6] B.J. Kooi, M.A.J. Somers, E.J. Mittenmeijer, Thermodynamics and Long-Range Order of Interstitials in a Hexagonal Close-Packed Lattice, Metall. Mater. Trans. A. 25 (1994) 2797–2814.

[7] A. Leineweber, H. Jacobs, Theoretical analysis of occupational ordering in hexagonal interstitial compounds: carbides, nitrides and oxides with "ε-type" superstructures, J. Alloys Compd. 308 (2000) 178–188.

[8] A. Leineweber, H. Jacobs, F. Hüning, H. Lueken, W. Kockelmann, Nitrogen ordering and ferromagnetic properties of ε-Fe_3N_{1+x} ($0.10 \leq x \leq 0.39$) and ε-$Fe_3(N_{0.80}C_{0.20})_{1.38}$, J. Alloys Compd. 316 (2001) 21–38.

[9] A. Leineweber, H. Jacobs, F. Hüning, H. Lueken, H. Schilder, W. Kockelmann, ε-Fe_3N: magnetic structure, magnetization and temperature dependent disorder of nitrogen, J. Alloys Compd. 288 (1999) 79–87.

[10] A. Leineweber, Mobility of nitrogen in ε-Fe_3N below 150°C: The activation energy for reordering, Acta Mater. 55 (2007) 6651–6658.

[11] H.A. Wriedt, N.A. Gokcen, R.H. Nafziger, The Fe-N (Iron-Nitrogen) System, Bull. Alloy Phase Diagrams. 8 (1987) 355–377.

[12] K.H. Eickel, W. Pitsch, Magnetic Properties of the Hexagonal Iron Nitride ε-$Fe_{3.2}N$, Phys. Status Solidi. 39 (1970) 121–129.

[13] P. Schaaf, K.-P. Lieb, E. Carpene, M. Han, F. Landry, Laser-produced iron nitrides seen by Mössbauer spectroscopy, Czechoslov. J. Phys. 51 (2001) 625–650.

[14] G.M. Chen, N.K. Jaggi, J.B. Butt, E.B. Yeh, L.H. Schwartz, Mössbauer and Magnetic Studies of ε-Fe_xN, $2 < x < 3$, J. Phys. Chem. 87 (1983) 5326–5332.

[15] M.A.J. Somers, B.J. Kooi, L. Maldzinski, E.J. Mittemeijer, A.A. van der Horst, A.M. van der Kraan, et al., Thermodynamics and long-range order of interstitials in an h.c.p. lattice: Nitrogen in ε-Fe_2N_{1-z}, Acta Mater. 45 (1997) 2013–2025.

[16] S. Shang, A.J. Böttger, M.P. Steenvoorden, M.W.J. Crajé, Hyperfine interactions

in hexagonal ε-Fe_6N_y phase investigated by Mössbauer spectroscopy and ab initio calculations, Acta Mater. 54 (2006) 2407–2417.

[17] K.H. Jack, Binary and Ternary Interstitial Alloys. II. The Iron-Carbon-Nitrogen System, Proc. R. Soc. London A. 195 (1948) 41–55.

[18] F.K. Naumann, G.L. Langenscheid, Beitrag zum System Eisen-Stickstoff-Kohlenstoff, Arch. Eisenhüttenwes. 36 (1965) 677–682.

[19] V.F. Sears, Neutron scattering lengths and cross sections, Neutron News. 3 (1992) 26–37.

[20] Z.Q. Liu, A. Leineweber, E.J. Mittemeijer, K. Mitsuishi, K. Furuya, Electron-diffraction study on ε-iron nitride powders with various nitrogen contents: Variation of long-range nitrogen ordering, J. Mater. Res. 21 (2006) 2572–2581.

[21] J.T. Slycke, E.J. Mittemeijer, M.A.J. Somers, In: E.J. Mittemeijer, M.A.J. Somers (Editors), Thermochemical Surface Engineering of Steels, Woodhead Publishing, Cambridge, UK, 2015: pp. 3–111.

[22] J. Chao, B.J. Zwolinski, Ideal gas thermodynamic properties of ethylene and propylene, J. Phys. Chem. Ref. Data. 4 (1975) 251–261.

[23] R.C. Wimpory, P. Mikula, J. Šaroun, T. Poeste, J. Li, M. Hofmann, et al., Efficiency Boost of the Materials Science Diffractometer E3 at BENSC: One Order of Magnitude Due to a Horizontally and Vertically Focusing Monochromator, Neutron News. 19 (2008) 16–19.

[24] R.J. Hill, C.J. Howard, LHPM. A Computer Program for Rietveld Analysis of Fixed-Wavelength X-ray and Neutron Powder Diffraction Patterns, AAEC (Now ANSTO) Rep. M112. (1986) Lucas Heights Research Laboratory, Australia.

[25] K. Fabian, V.P. Shcherbakov, S.A. McEnroe, Measuring the Curie temperature, Geochemistry, Geophys. Geosystems. 14 (2013) 947–961.

[26] R.J. Bouchard, C.G. Frederick, V. Johnson, Preparation and properties of submicron hexagonal Fe_xN, $2<x<3$, J. Appl. Phys. 45 (1974) 4067–4070.

[27] M. Kano, T. Nakagawa, T.A. Yamamoto, M. Katsura, Magnetism, crystal structure and nitrogen content near the ε-ζ phase boundary of iron nitrides, J. Alloys Compd. 327 (2001) 43–46.

[28] M. Sifkovits, H. Smolinski, S. Hellwig, W. Weber, Interplay of Chemical Bonding and Magnetism in Fe_4N, Fe_3N and Fe_2N, J. Magn. Magn. Mater. 204 (1999) 191–198.

[29] C.M. Fang, M.A. van Huis, J. Jansen, H.W. Zandbergen, Role of carbon and nitrogen in Fe_2C and Fe_2N from first-principles calculations, Phys. Rev. B. 84 (2011) 094102.

[30] J. Chen, C. Yu, H. Lu, Phase stability, magnetism, elastic properties and hardness of binary iron nitrides from first principles, J. Alloys Compd. 625 (2015) 224–230.

[31] G. Li, Y. Liu, R. Zhao, J. Shen, S. Wang, P. Shan, et al., Crystallographic phases and magnetic properties of iron nitride films, Thin Solid Films. 589 (2015) 22–26.

[32] P. Schaaf, C. Illgner, M. Niederdrenk, K.P. Lieb, Characterization of laser-nitrided iron and sputtered iron nitride films, Hyperfine Interact. 95 (1995) 199–225.

[33] M. Niederdrenk, P. Schaaf, K.-P. Lieb, O. Schulte, Characterization of magnetron-sputtered ε iron-nitride films, J. Alloys Compd. 237 (1996) 81–88.

[34] A. V. dos Santos, C.A.S. Pérez, Ab initio investigation of the substitution effects of 2p elements on the electronic structure of γ-Fe_4X (X = B, C, N, and O) in the ground state, J. Mater. Res. 31 (2016) 202–212.

[35] T. Liapina, A. Leineweber, E.J. Mittemeijer, W. Kockelmann, The lattice parameters of ε-iron nitrides: Lattice strains due to a varying degree of nitrogen ordering, Acta Mater. 52 (2004) 173–180.

[36] M. Robbins, J.G. White, Magnetic properties of epsilon-iron nitride, J. Phys. Chem. Solids. 25 (1964) 717–720.

[37] H.N. Fang, R. Zhang, B. Liu, Z.K. Tao, M.W. Xiao, X.F. Wang, et al., Analysis of magnetic structures of iron nitrides by Landau's theory of second-order phase transitions, AIP Adv. 3 (2013) 072136.1–9.

[38] B.K. Brink, K. Ståhl, T.L. Christiansen, M.A.J. Somers, The ternary Fe-C-N system: Homogeneous distributions of nitrogen and carbon, J. Alloys Compd. Accepted (2016).

[39] D. Firrao, B. DeBenedetti, M. Rosso, Sugli strati superficiali di acciai trattati in bagni salini a base di cianati e carbonati alcalini, Met. Ital. 71 (1979) 373–381.

[40] L. Cheng, A. Böttger, E.J. Mittemeijer, Tempering of Iron-Carbon-Nitrogen Martensites, Metall. Mater. Trans. A. 23 (1992) 1129–1145.

[41] A. Böttger, M.J. van Genderen, S.J. Sijbrandij, E.J. Mittemeijer, G.D.W. Smith, Atom-probe- and X-ray Diffraction Analysis of the Composition and Structure of Precipitates Formed on Tempering of Ternary Iron-Carbon-Nitrogen Martensites, ISIJ Int. 36 (1996) 764–767.

[42] A. Leineweber, H. Jacobs, W. Kockelmann, S. Hull, D. Hinz-Hübner, High temperature axial ratios c/a in hcp-based ε-type interstitial nitrides MN_y with M = Mn, Fe, Ni, J. Alloys Compd. 384 (2004) 1–5.

[43] M.I. Pekelharing, A. Böttger, M.A.J. Somers, M.P. Steenvoorden, A.M. van der Kraan, E.J. Mittemeijer, Modeling Thermodynamics of Fe-N Phases: Characterisation of ε-Fe_2N_{1-z}, Mater. Sci. Forum. 318-320 (1999) 115–120.

Fig. 1: Octahedral interstitial positions denoted A1-C2 (light spheres) in an h.c.p. structure of Fe atoms (dark spheres).

Fig. 2: *a*) Magnetic hysteresis curves for ε-iron (carbo)nitrides at 80 K and *b*) specific magnetization versus temperature at B_0 = 0.05 T measured at a cooling rate of 1.5 K/min. For clarity only every 30th measurement point is shown, except for the inset in *a*).

Fig. 3: Curie temperature (T_C) obtained for ε-Fe_2N_{1-z} and ε-$Fe_2(N,C)_{1-z}$ compared to the values obtained for ε-Fe_2N_{1-z} by Leineweber *et al.* [8], Kano *et al.* [27] and Bouchard *et al.* [26]. A solid line is drawn connecting the two pure nitride samples to emphasize the increased T_C of the carbonitrides, for which the trend is indicated as a dashed line.

Fig. 4: Mössbauer spectra of ε-iron (carbo)nitrides recorded at 18 K. Data are presented as points, fits as black lines and the individual sextet components as grey lines with shaded areas.

Fig. 5: Hyperfine fields (B_{hf}) and isomer shifts (δ) for ε-Fe_2N_{1-z} and ε-$Fe_2(N,C)_{1-z}$ at 18 K compared to the values obtained for ε-Fe_2N_{1-z} by Chen *et al.* [14], Somers *et al.* [15] and Pekelharing *et al.* [43] at 4.2 K. Dashed lines are drawn to guide the eye and emphasize the deviation between trends for nitrides (solid) and carbonitrides (dashed) for components II and IIIa.

Fig. 6: Neutron diffractogram (MEREDIT diffractometer, λ = 1.46 Å), refined Rietveld profile and difference curve for *a*) $Fe_2(N_{0.706}C_{0.294})_{0.92}$ and *b*) $Fe_2(N_{0.715}C_{0.285})_{0.92}$. Comparison of superstructure reflections of structural models in space group $P\bar{3}1m$ (*c*+*d*) and $P6_322$ (*e*+*f*) for $Fe_2(N_{0.715}C_{0.285})_{0.92}$. Note the $^{\lambda}/_{2}$-contribution (intensity ratio 0.004).

Fig. 7: Lattice parameters (*a* and *c*) versus temperature for ε-iron (carbo)nitrides. Estimated standard deviations are ≤ 10^{-3} Å. Lines correspond to the fitted expression for thermal expansion.

Fig. 8: *a*) Lattice parameters versus interstitial content for ε-$Fe_2(N_{1-x}C_x)_{1-z}$ (solid symbols) compared to additional values obtained with X-ray diffraction [38] (open symbols) and published relations for pure nitrides by Somers *et al.* [15] and Liapina *et al.* [35] and for carbonitrides by Firrao *et al.* [39]. Labels denote the fraction of interstitial carbon atoms, *x*. *b*) The difference in lattice parameter *c* and the published relation [15] for ε-nitrides ($\Delta c = c - c(z)$) plotted versus the carbon content, *x*. The solid line corresponds to the fitted relation including correction for carbon content ($\Delta c = c(z,x) - c(z) = -0.057x$) obtained from equation 1 and the dashed line ($\Delta c = 0$) corresponds to a theoretical constant lattice parameter not affected by substitution of nitrogen by carbon

Fig. 9: Ratio of thermal expansion coefficients α(*c*)/α(*a*) for ε-$Fe_2(N_{1-x}C_x)_{1-z}$. Labels denote the fraction of interstitial carbon atoms, *x*. Current values obtained with neutron diffraction (solid symbols) are compared to additional values obtained with X-ray diffraction [38] (open symbols).

Graphical Abstract (for review)

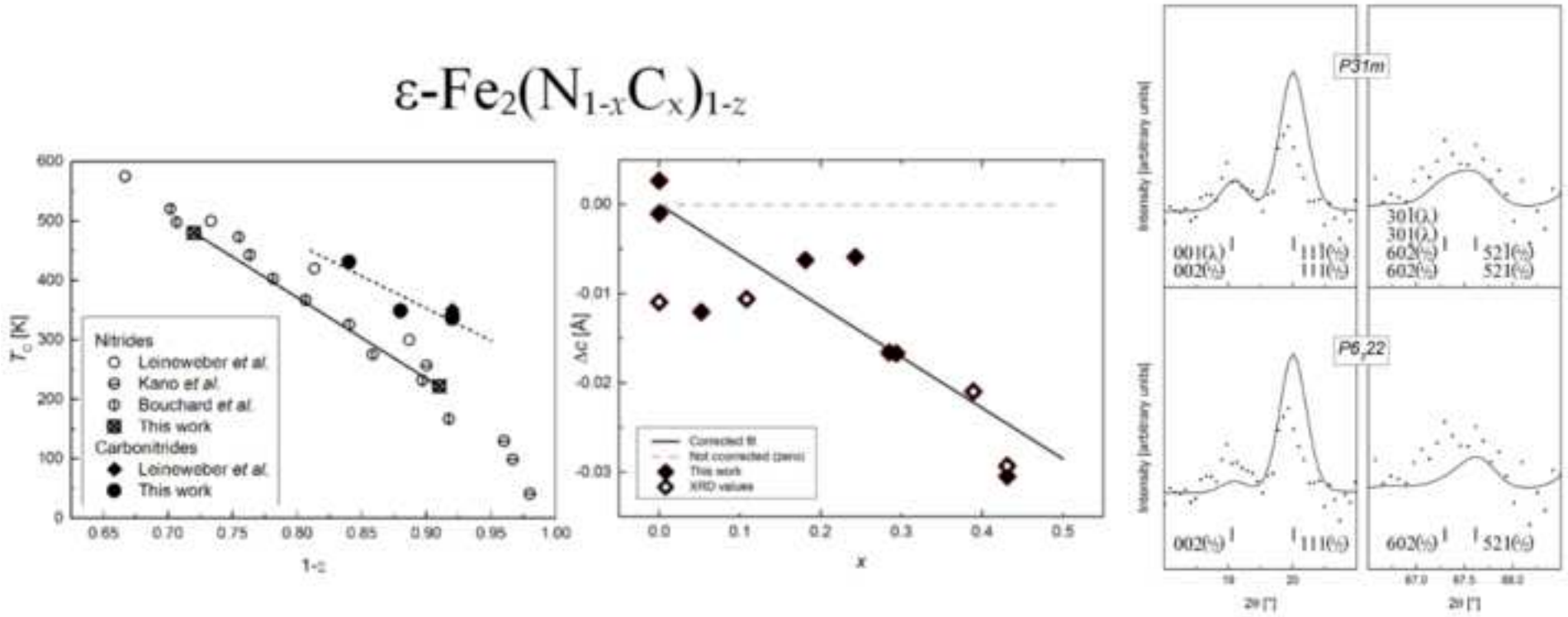

Highlights:

- The effects of substitution of nitrogen by carbon in ε-$Fe_2(N_{1-x}C_x)_{1-z}$ are explored.
- Partial substitution affects magnetic properties and interstitial ordering.
- The Curie temperature, saturation magnetization and hyperfine fields are increased.
- Isomer shifts and the *c* lattice parameter are decreased.
- Changes in ordering are related to relatively favorable interactions between N and C.

Figure 1

Click here to download high resolution image

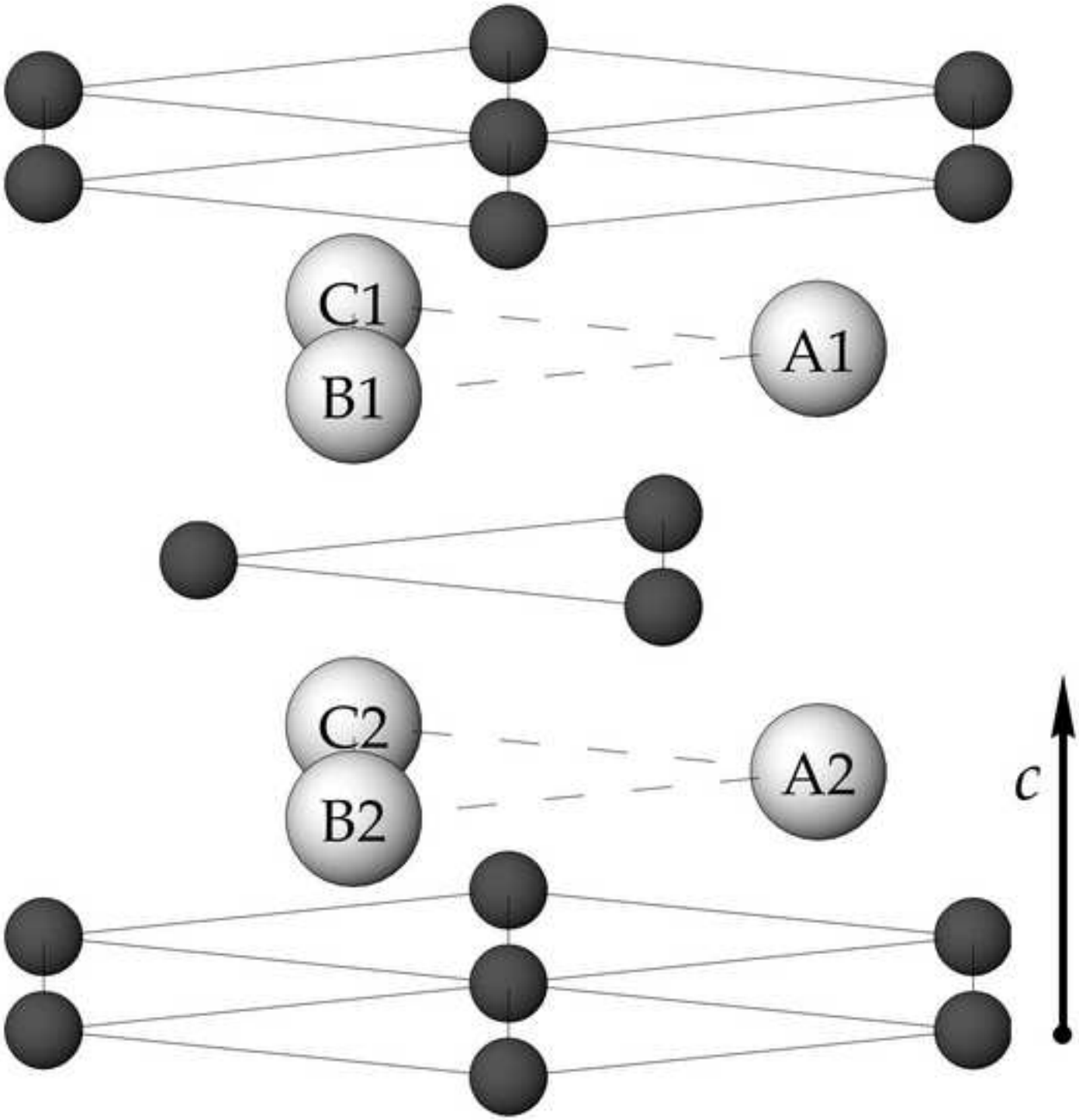

Figure 2

Click here to download high resolution image

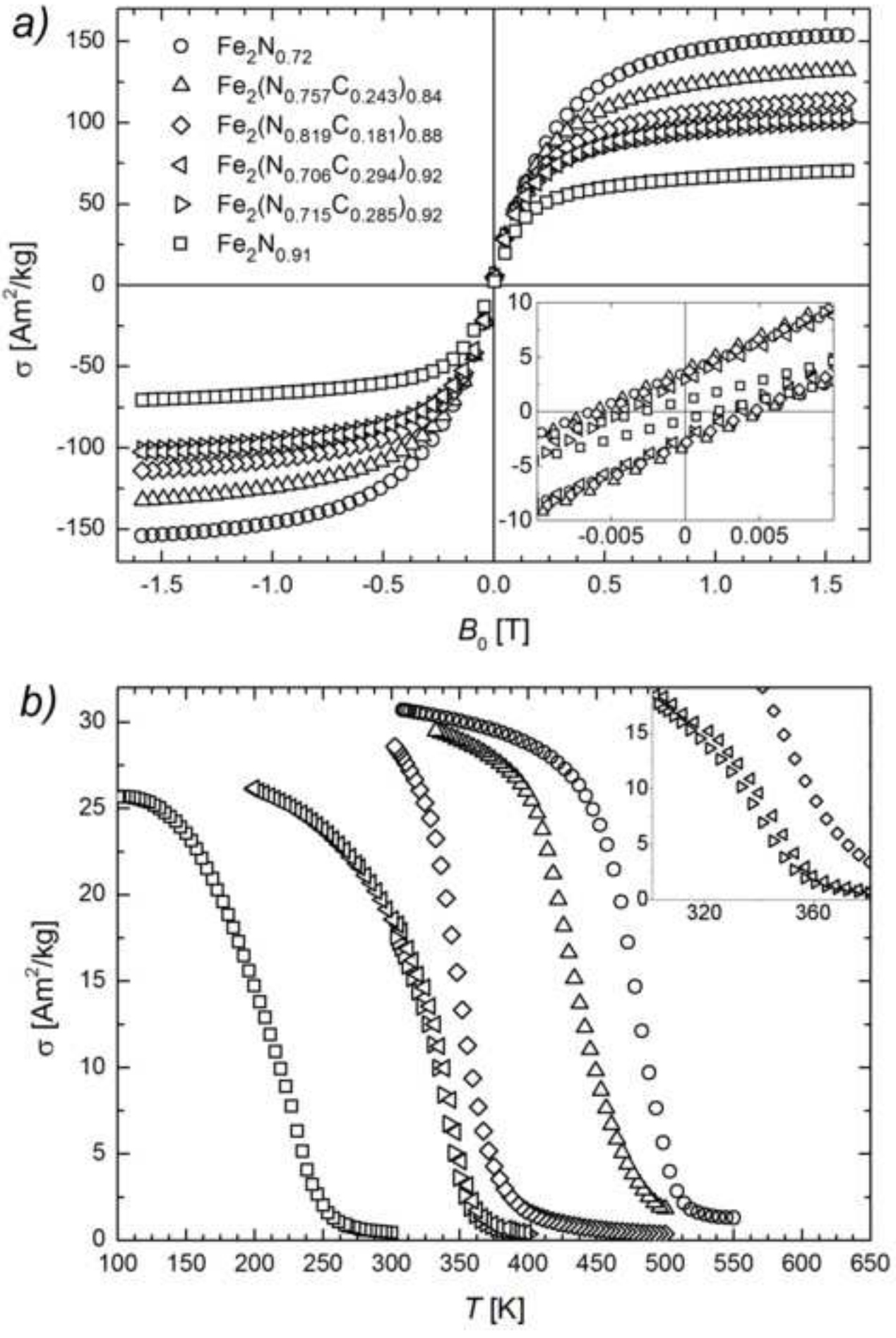

Figure 3

Click here to download high resolution image

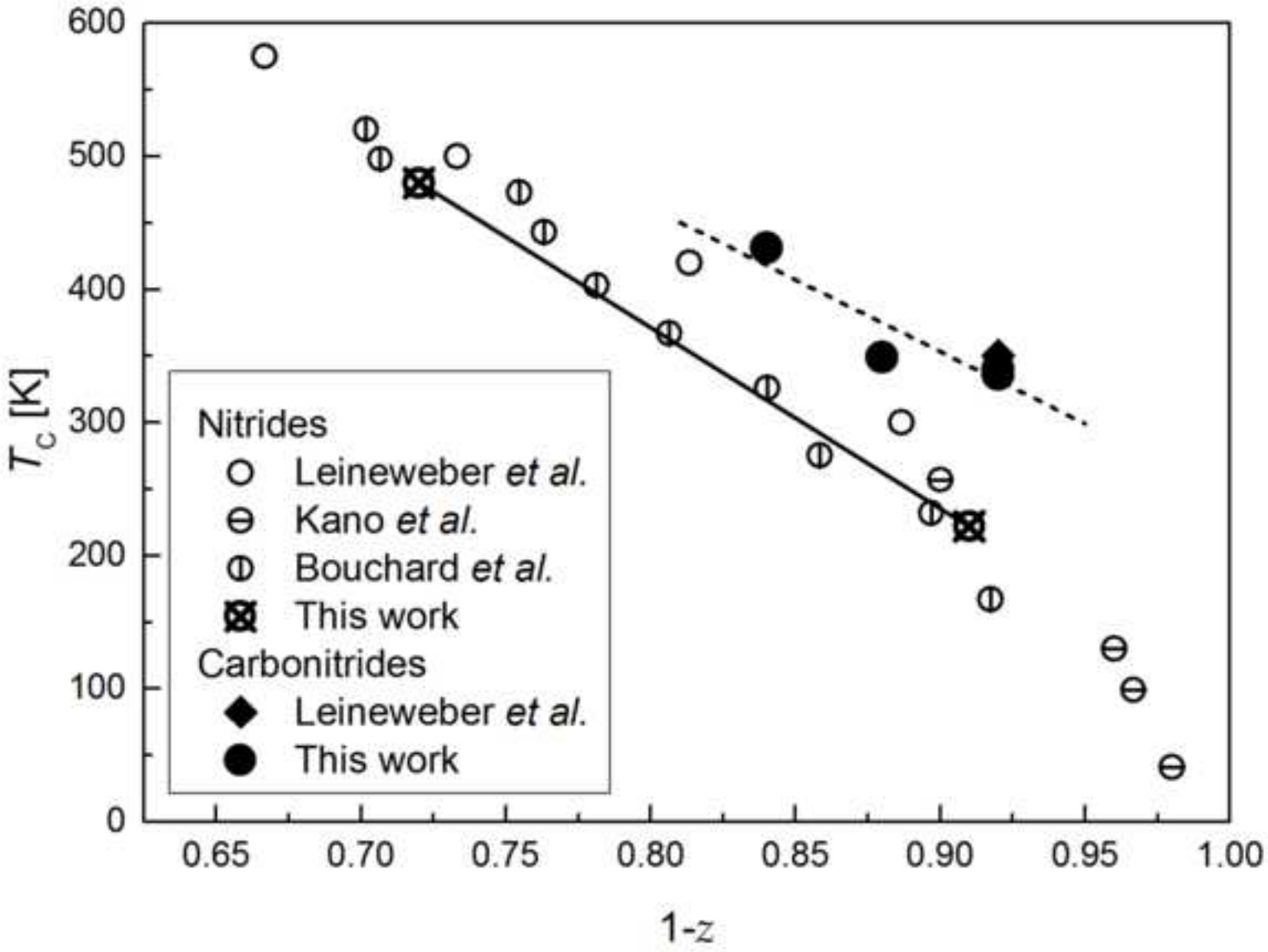

Figure 4

Click here to download high resolution image

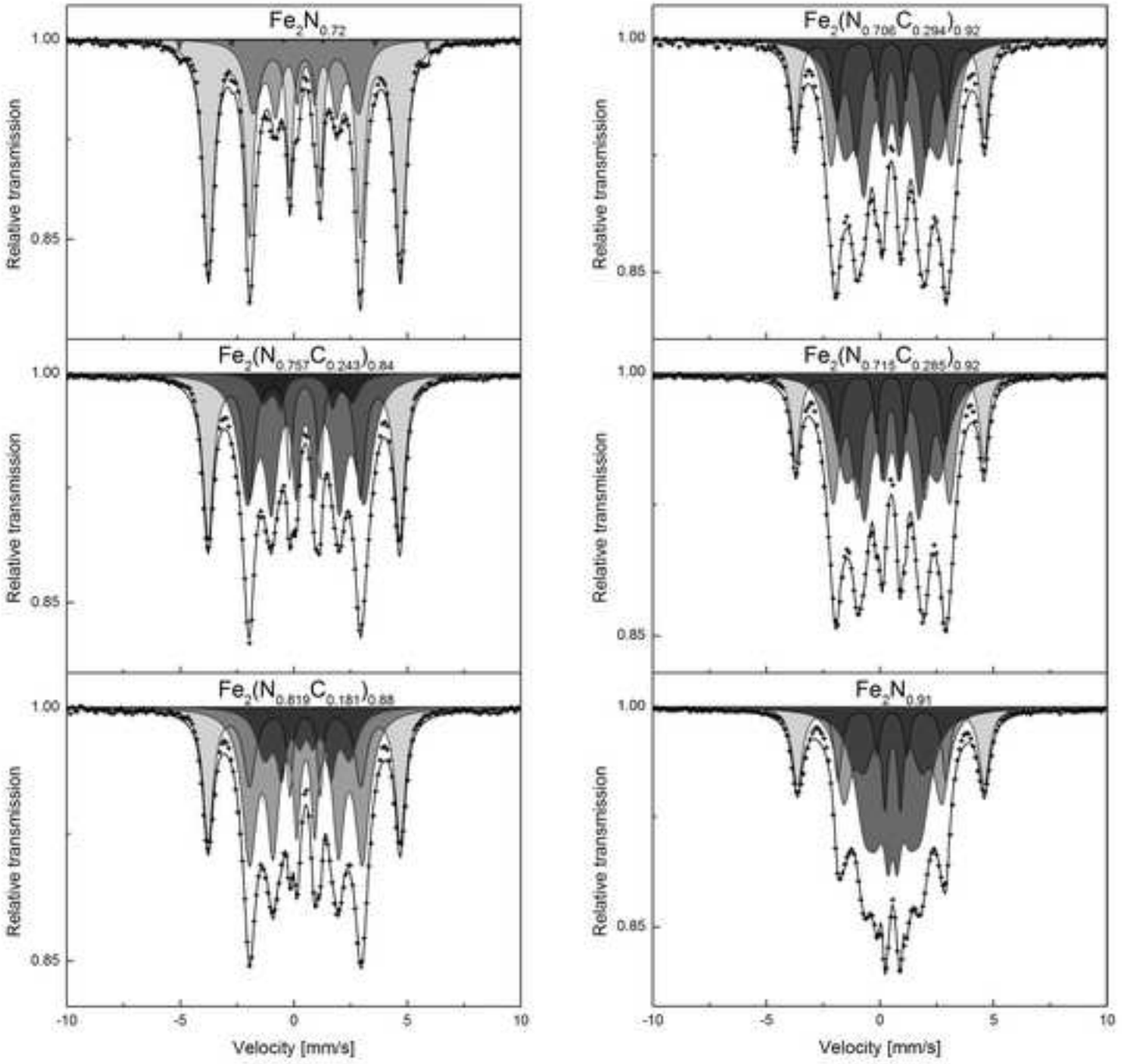

Figure 5

Click here to download high resolution image

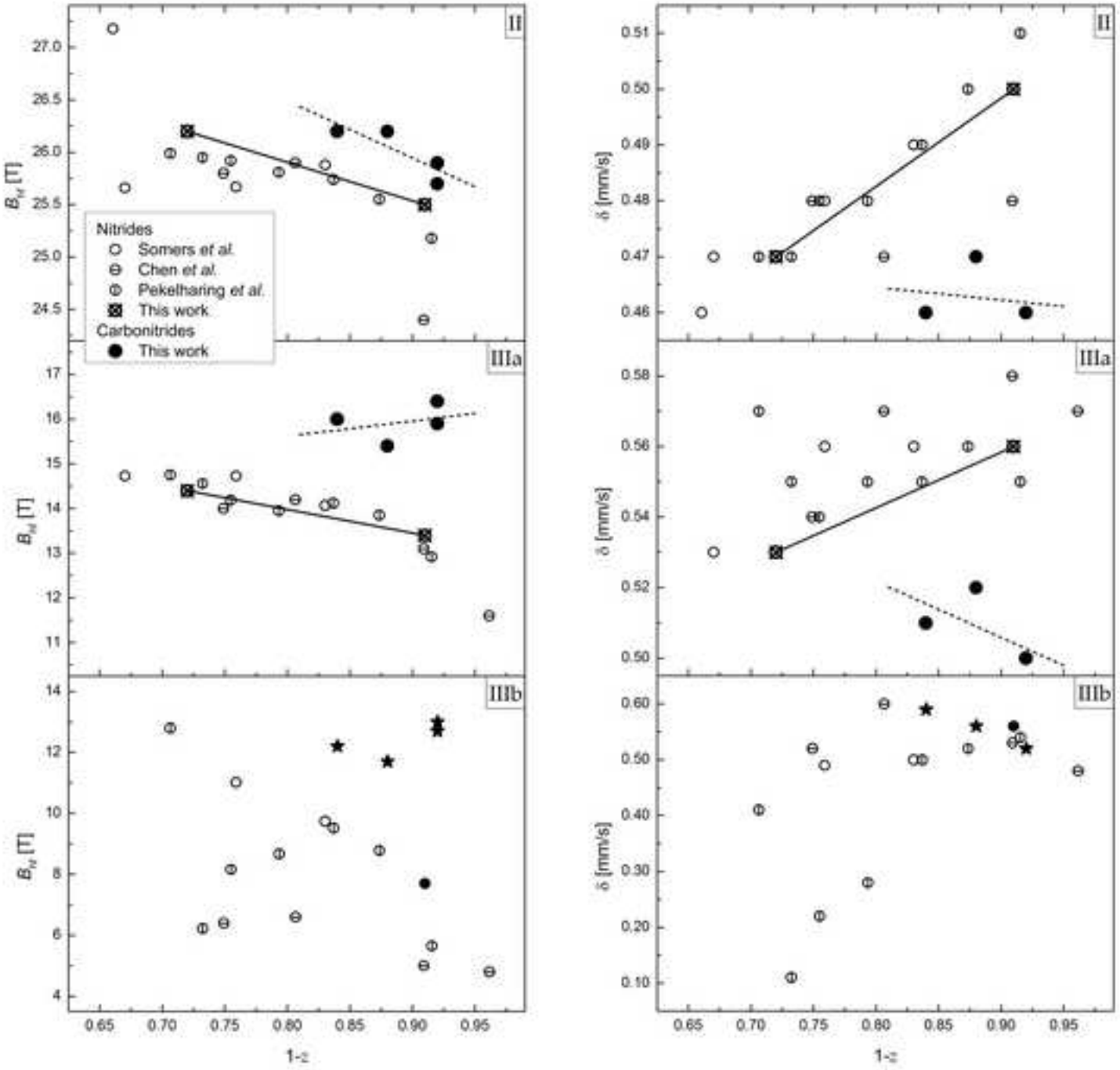

Figure 6

Click here to download high resolution image

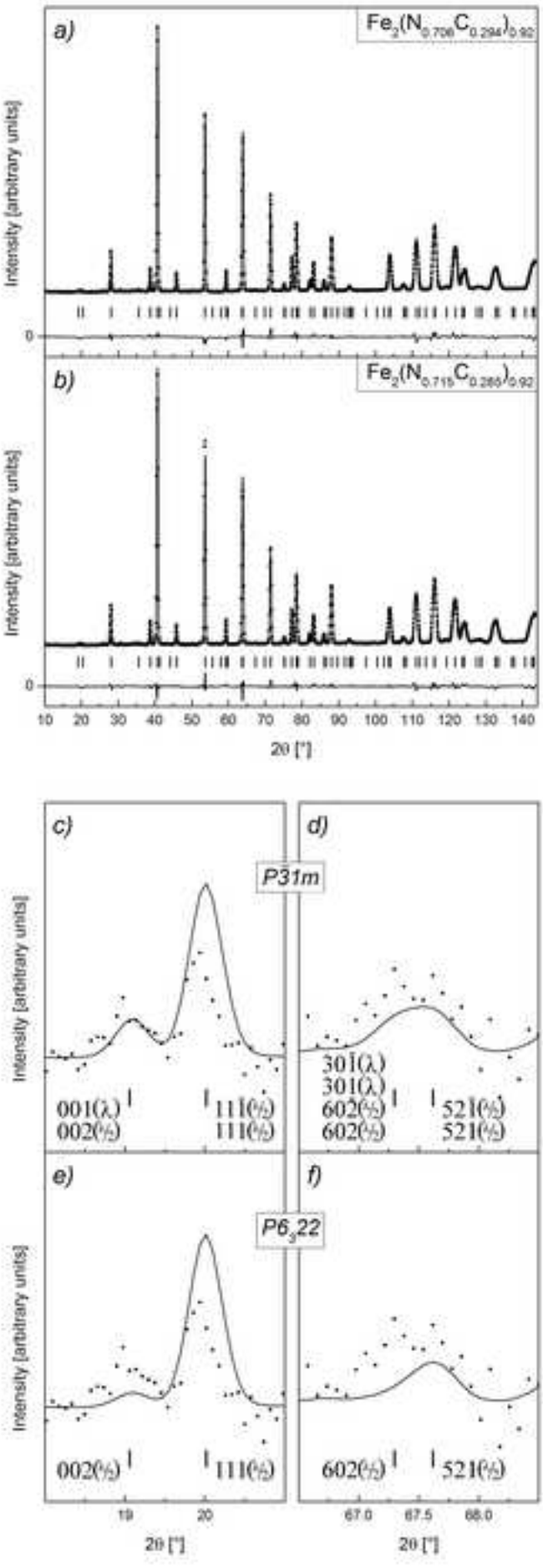

Figure 7

Click here to download high resolution image

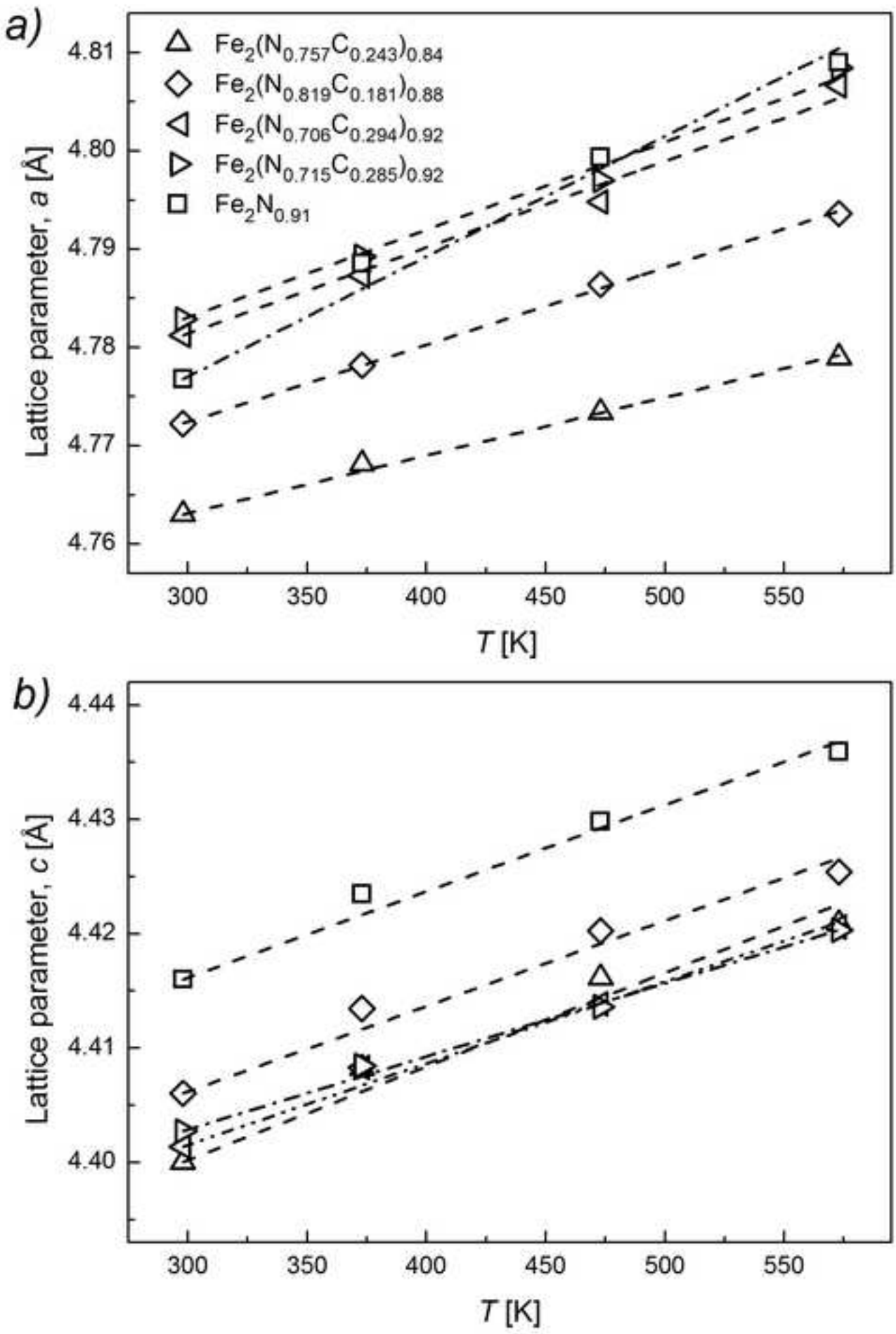

Figure 8

Click here to download high resolution image

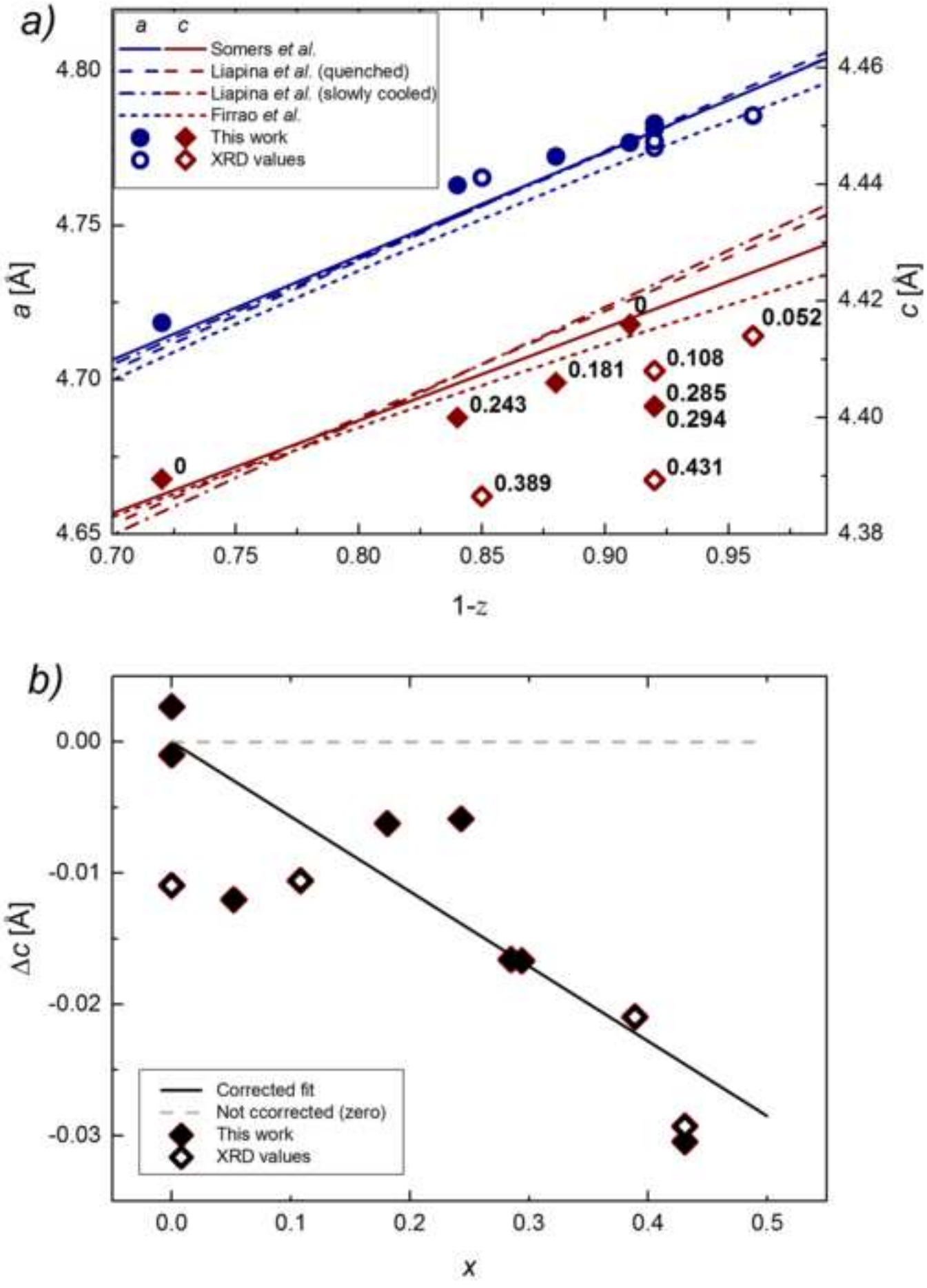

Figure 9
Click here to download high resolution image